APPLIED PHYSICS LETTERS **91**, 063125 (2007)

Visibility of graphene flakes on a dielectric substrate

D. S. L. Abergel,[a] A. Russell, and Vladimir I. Fal'ko
Physics Department, Lancaster University, Lancaster LA1 4YB, United Kingdom

(Received 3 May 2007; accepted 11 July 2007; published online 10 August 2007)

The authors model the optical visibility of monolayer and bilayer graphene deposited on a SiO_2/Si substrate or thermally annealed on the surface of SiC. Visibility is much stonger in reflection than in transmission, reaching the optimum conditions when the bare substrate transmits light resonantly. In the optical range of frequencies a bilayer is approximately twice as visible as a monolayer thereby making the two types of graphene distinguishable from each other. © *2007 American Institute of Physics*. [DOI: 10.1063/1.2768625]

Monolayer graphene is a single two-dimensional honeycomb lattice of carbon atoms. Although the first graphene-based structures were only recently fabricated[1] they have quickly become the subject of an extensive research effort.[2–4] Monolayer graphene is a zero-gap semiconductor with a Dirac-like dispersion of chiral quasiparticles near the K points of the hexagonal first Brillouin zone.[5] Bilayer graphene is a pair of graphene sheets with the Bernal (AB) stacking arrangement. In the low-energy spectrum of this material[6] the conduction and valence bands both consist of two quadratic branches split by the interlayer coupling γ_1. Measurements of the quantum Hall effect[1,2,7] and angle-resolved photoemission spectroscopy experiments[8] have confirmed that these are the low-energy band structures of these materials.

The widespread microcleavage technique used to fabricate graphene-based devices requires a visual inspection of the substrate[1] to find flakes of one or two layers thickness. In this letter, we aim to determine the optimum conditions for making these flakes optically visible when they are deposited on various substrates. The parameters at one's disposal (see Fig. 1) are the frequency ω, angle $\bar{\alpha}$, and aperture $\delta\alpha$ of the focused incident radiation, as well as the thicknesses of the various layers of the underlying dielectric materials.

Below we calculate the reflection of nonpolarized incident light taking the geometry of the substrate into account with suitable boundary conditions at each of the interfaces between materials, appropriate frequency-dependent dielectric functions $\varepsilon(\omega)$ for each layer, and $\mu=1$. For numerical analysis, we use the data[9] available in the existing literature for the dispersion of the permittivity of silicon,[10] silicon oxide,[11] and silicon carbide.[12] With reference to Fig. 1, we analyze the reflection R of light from a substrate with a flake on it and compare this to the reflection R_0 of a bare (graphene-free) substrate. The optical visibility of a flake is then determined as the contrast between two such parts of the sample studied using a monochromatic light source,

$$V_R = (R - R_0)/R_0. \tag{1}$$

The scattering of light is analyzed using the electromagnetic wave equations in vacuum and dielectric media and the standard boundary conditions at interfaces between different materials,

$$\mathbf{E}_1^{\parallel} = \mathbf{E}_2^{\parallel},$$

$$\mathbf{D}_1^{\perp} = \mathbf{D}_2^{\perp},$$

$$\mathbf{B}_1^{\parallel} - \mathbf{B}_2^{\parallel} = \sigma(\omega)\mathbf{E} \times \mathbf{n}. \tag{2}$$

The superscripts $\parallel$ and $\perp$ stand for the components of the field parallel and perpendicular to the interface, respectively, $\mathbf{n}$ is the unit vector normal to the interface, the subscript 1 (2) denotes the field below (above) the interface, $\sigma(\omega)$ is the frequency-dependent conductivity of a graphene flake, and $\mathbf{D}=\epsilon(\omega)\mathbf{E}$. One more boundary condition (on the perpendicular components of $\mathbf{H}$) duplicates Snell's law.

Having in mind an optical setup used to locate a small flake, we consider a beam of light focused by a lens, so that the light in the beam arrives at the substrate surface with some aperture $\delta\alpha$ (see Fig. 1). Therefore the measurable reflectance to be used in Eq. (1) is

$$R(\bar{\alpha}, \delta\alpha) = \int d\Omega_{\mathbf{k}} R(\mathbf{k}) P(\mathbf{k}), \tag{3}$$

where $P(\mathbf{k})$ characterizes the spread of the beam over the solid angle of the aperture $\delta\alpha$ around $\bar{\alpha}$, $\mathbf{k}$ is the wave vector of the incident ray of light, and $R(\mathbf{k})$ is the reflection coefficient for a plane wave with this wave vector. Below we assume that the beam is equally dense at all angles within an aperture of $\delta\alpha$ around $\bar{\alpha}$.

To describe the conductivity of graphene, we follow the method used in Refs. 13 and 14 taking into account the split bands formed in the bilayer.[6] At low temperatures the result

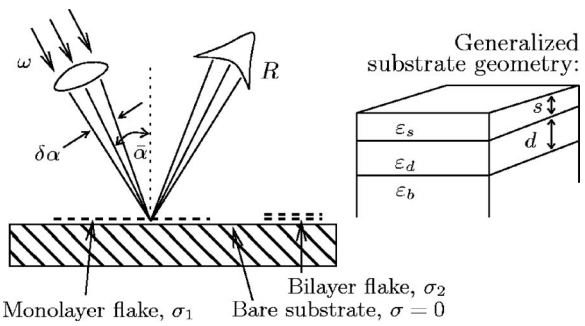

FIG. 1. Geometrical configuration for detection of graphene on a substrate. A light beam is focused on a small spot which is scanned along the surface. The calculations presented below show how to optimize the conditions for visibility of atomically thin graphitic flakes.

[a]Electronic mail: daveabergel@googlemail.com

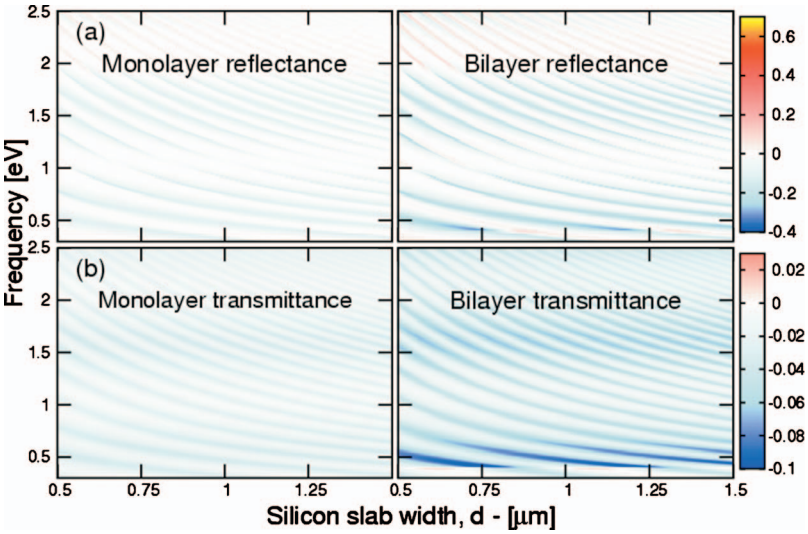

FIG. 2. (Color) Visibility in (a) reflectance V_R and (b) transmittance V_T for graphene on a silicon wafer with a 300 nm oxide layer for varying substrate thickness and frequency of radiation. Note the difference in the scales of (a) and (b). Here we take an aperture of $\delta\alpha=10°$ and $\bar{\alpha}=20°$.

for the monolayer which takes into account the transition between the valence and conduction bands in the Dirac spectrum is $\sigma_1=e^2/4\hbar$ (with a negligible imaginary part).[13] This corresponds[15] to the absorption coefficient $g=4\pi\sigma/c$ which gives $g_1=\pi e^2/\hbar c\approx 2.5\%$. For the bilayer, there are four possible interband transitions, reflected by its conductivity,

$$\sigma_2=\frac{e^2}{2\hbar}\left(\frac{1}{2}\frac{\Omega+2}{\Omega+1}+\frac{1}{\Omega^2}\theta(\Omega-1)+\frac{1}{2}\frac{\Omega-2}{\Omega-1}\theta(\Omega-2)\right)+i\frac{e^2}{2\pi\hbar}\left(\frac{\Omega}{1-\Omega^2}\log\Omega+\frac{2}{\Omega}-\frac{1}{\Omega^2}\log\left|\frac{1+\Omega}{1-\Omega}\right|-\frac{1}{2}\frac{\Omega^2-2}{\Omega^2-1}\log\left|\frac{2+\Omega}{2-\Omega}\right|-\frac{1}{2}\frac{\Omega}{\Omega^2-1}\log|4-\Omega^2|\right). \tag{4}$$

Here $\Omega=\hbar\omega/\gamma_1$ is the frequency written in units of the interlayer coupling and $\theta(x)=[1+\mathrm{sgn}(x)]/2$. The real part of this function has a discontinuity at $\hbar\omega=\gamma_1\approx 0.4$ eV and a cusp at $\hbar\omega=2\gamma_1$. These correspond to the activation (at zero temperature) of the interband transitions between low-energy bands and split bands, and the two split bands, respectively. The imaginary part of σ_2 shows a divergency at $\hbar\omega=\gamma_1$, leading to an enhanced reflectance of the bilayer at this frequency.

For nonpolarized light arriving at the incidence angle α to the sample depicted on the right-hand side of Fig. 1 with graphene deposited on the top surface, the reflectance is

$$R=\frac{1}{2}\left|\frac{\sqrt{\varepsilon_s}\cos\alpha_s D-(\cos\alpha-(4\pi\sigma/c))C}{\sqrt{\varepsilon_s}\cos\alpha_s D+(\cos\alpha+(4\pi\sigma/c))C}\right|^2+\frac{1}{2}\left|\frac{\sqrt{\varepsilon_s}\cos\alpha C'-\cos\alpha_s D'(1-(4\pi\sigma/c)\cos\alpha)}{\sqrt{\varepsilon_s}\cos\alpha C'+\cos\alpha_s D'(1+(4\pi\sigma/c)\cos\alpha)}\right|^2. \tag{5}$$

In this result, the first term represents reflection of radiation polarised so that the electric field is perpendicular to the plane of incidence, the second term to radiation polarised so that the electric field is parallel to the plane of incidence and

$$A=-\sqrt{\varepsilon_d}\cos\alpha_d\cos X_d+i\sqrt{\varepsilon_b}\cos\alpha_b\sin X_d,$$

$$B=i\sqrt{\varepsilon_d}\cos\alpha_d\cos X_d-\sqrt{\varepsilon_b}\cos\alpha_b\cos X_d,$$

$$C=-i\sqrt{\varepsilon_d}\cos\alpha_d B\sin X_s+\sqrt{\varepsilon_s}\cos\alpha_s A\cos X_s,$$

$$D=\sqrt{\varepsilon_d}\cos\alpha_d B\cos X_s-i\sqrt{\varepsilon_s}\cos\alpha_s A\sin X_s,$$

$$A'=\sqrt{\varepsilon_b}\cos\alpha_d\cos X_d-i\sqrt{\varepsilon_d}\cos\alpha_b\sin X_d,$$

$$B'=\sqrt{\varepsilon_d}\cos\alpha_b\cos X_d-i\sqrt{\varepsilon_b}\cos\alpha_d\sin X_d,$$

$$C'=\sqrt{\varepsilon_d}\cos\alpha_s A'\cos X_s-i\sqrt{\varepsilon_s}\cos\alpha_d B'\sin X_s,$$

$$D'=-i\sqrt{\varepsilon_d}\cos\alpha_s A'\sin X_s+\sqrt{\varepsilon_s}\cos\alpha_d B'\cos X_s.$$

Here $X_s=\sqrt{\varepsilon_s}ks\cos\alpha_s$, $X_d=\sqrt{\varepsilon_d}kd\cos\alpha_d$, $\sin\alpha_b=\sin\alpha/\sqrt{\varepsilon_b}$, $\sin\alpha_s=\sin\alpha/\sqrt{\varepsilon_s}$, and $\sin\alpha_d=\sin\alpha/\sqrt{\varepsilon_d}$. The angle α is determined by the direction of the wave vector of the incident plane wave, see Fig. 1. To model a finite slab of silicon of width d with a silicon oxide layer of width s on top, we substitute $\varepsilon_d=\varepsilon_{\mathrm{Si}}(\omega)$, $\varepsilon_s=\varepsilon_{\mathrm{SiO_2}}$, $\varepsilon_b=1$, and the quantity R_0 is found by replacing $\sigma=0$ in these expressions. To evaluate the visibility V_R, the integral in Eq. (3) must be taken for R and R_0 using Eq. (5).

Figure 2 illustrates the visibility of mono- and bilayer flakes on a Si substrate of widths $0.5\ \mu\mathrm{m}<d<1.5\ \mu\mathrm{m}$ and a 300 nm SiO_2 layer (see Fig. 1) for light with $0.3\ \mathrm{eV}<\hbar\omega<2.5$ eV arriving with aperture $\delta\alpha=10°$ around $\bar{\alpha}=20°$. The rapid oscillations of the visibility in this plot are caused by the resonant condition of the Si layer. When this layer is strongly transmitting (that is, when $\cos X_d\approx 0$), the visibility is at its highest. This fine structure is modulated by the corresponding resonance condition in the oxide which is responsible for the "bands" which lie across the plots in Fig. 2. The condition for maximum transmission through the oxide is $\cos X_s\approx 0$ which leads to

$$\omega\approx c\left(n+\tfrac{1}{2}\right)\pi/(s\sqrt{\varepsilon_s}\cos\alpha_s), \tag{6}$$

where n is an integer. The wave vector of the light in the slab is of the order of an inverse micron, so the resonant conditions are closely spaced on the length scale of the substrate thickness. The visibility of a bilayer flake is higher than the visibility of a monolayer for $\hbar\omega>\gamma_1\approx 0.4$ eV because the conductivity of the bilayer is essentially twice as large as the conductivity of the monolayer in this energy range. Additionally, the divergency in the imaginary part of the bilayer con-

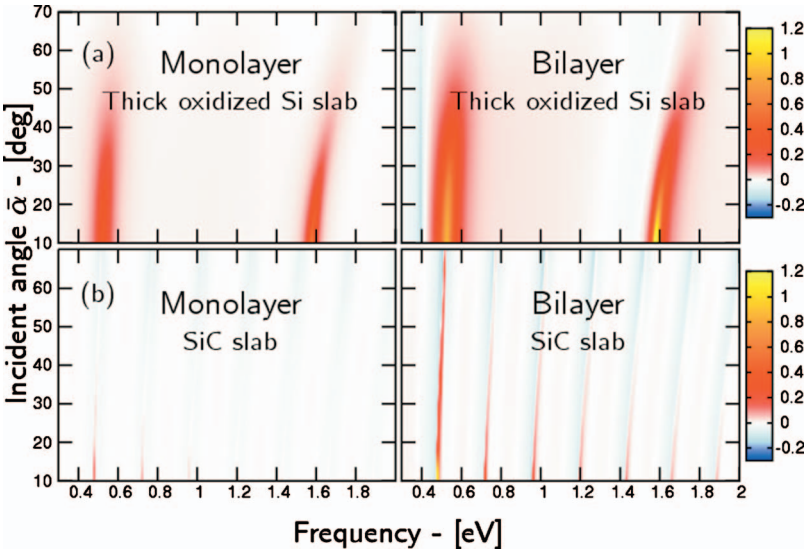

FIG. 3. (Color) Frequency dependence of visibility V_R of graphene on (a) an infinite silicon slab with a thin oxide layer of width 300 nm, and (b) a silicon carbide slab of width 1 μm. In both plots we use aperture $\delta\alpha = 10°$.

ductivity at $\hbar\omega = \gamma_1 \approx 0.4$ eV causes a stronger reflection and hence a larger visibility. Also we have calculated the transmittance T of the sample, and the corresponding visiblity $V_T = (T - T_0)/T_0$ is shown in Fig. 2(b) where the same resonant structure appears, but is at least ten times weaker than the visibility in reflectance.

We find that the visibility of graphene in reflectance is futher enhanced by using a thick (semi-infinite) substrate with a sizeable oxide layer on its surface, in agreement with a recent experimental observation.[16] Figure 3(a) shows the visibility of graphene deposited on a semi-infinite slab of silicon[9] with a 300 nm SiO_2 layer. In this case the analytical expression for the reflectance of a plane wave with wave vector $\mathbf{k} = (\omega/c)(\sin\alpha, 0, -\cos\alpha)$ can be found by substituting $\varepsilon_b = \varepsilon_{Si}(\omega)$, $\varepsilon_s = \varepsilon_{SiO_2}$ and $d = 0$ into Eq. (5). As before, both $R(\mathbf{k})$ and $R_0(\mathbf{k})$ (which is determined from this equation with $\sigma = 0$) must be substituted in Eq. (3) before the visibility is evaluated. In the plots in Fig. 3(a), the main features are the very strong reflectance of the graphene flake at $\hbar\omega \approx 0.5$ eV and $\hbar\omega \approx 1.6$ eV. These are due to the standing wave resonances in the oxide layer at the condition in Eq. (6). In Fig. 3(a) the peak in visibility at $\hbar\omega \approx 0.5$ eV $(n = 0)$ corresponds to the first resonance in the oxide layer and the peak at $\hbar\omega \approx 1.6$ eV $(n = 1)$ to the second resonance. The factor of 2 difference between the bilayer and monolayer conductivities at $\hbar\omega \gg \gamma_1$ and the divergence in the imaginary part of $\sigma_2(\omega)$ at $\hbar\omega = \gamma_1 \approx 0.4$ eV are manifested in the visibility.

Besides being produced using the microcleavage technique, ultrathin graphitic films can also be grown by thermal annealing of SiC wafers.[8,17] The reflectance for this configuration can be found by substituting[9] $d = 0$, $\varepsilon_b = 1$, and $\varepsilon_s = \varepsilon_{SiC}$ in Eq. (5). Plots of the visibility defined by this function are shown in Fig. 3(b). The standing wave resonance in the substrate is again the main factor for the visibility of graphene, though it is weaker for a SiC slab than for the SiO_2/Si substrates.

In conclusion, we have shown that graphene is much more visible in reflection than in transmission and that the resonance condition of the substrate is the dominating factor in determining its visibility. For optimum visibility the wavelength of monochromatic light used should be selected using Eq. (6), and for the visible frequency range (where $\sigma_2 \approx 2\sigma_1$) a bilayer is clearly distinguishable from a monolayer.

[1] K. S. Novoselov, A. K. Geim, S. V. Morozov, D. Jiang, Y. Zhang, S. V. Dubonos, I. V. Grigorieva, and A. A. Firsov, Science **306**, 666 (2004).
[2] K. S. Novoselov, A. K. Geim, S. V. Morozov, D. Jiang, M. I. Katsnelson, I. V. Grigorieva, and S. V. Dubonos, Nature (London) **438**, 197 (2005).
[3] Y. Zhang, J. P. Small, M. E. S. Amori, and P. Kim, Phys. Rev. Lett. **94**, 176803 (2005); Y. Zhang, Y. Tan, H. L. Stormer, and P. Kim, Nature (London) **438**, 201 (2005).
[4] A. Geim and K. Novoselov, Nat. Mater. **6**, 183 (2007).
[5] R. Saito, G. Dresselhaus and M. S. Dresselhaus, *Physical Properties of Carbon Nanotubes* (Imperial College, London, 1998), 28; T. Ando, J. Phys. Soc. Jpn. **74**, 777 (2005).
[6] E. McCann and V. I. Fal'ko, Phys. Rev. Lett. **96**, 086805 (2006).
[7] K. S. Novoselov, E. McCann, S. V. Morozov, V. I. Fal'ko, M. I. Katsnelson, U. Zeitler, D. Jiang, F. Schedin, and A. K. Geim, Nat. Phys. **2**, 177 (2006).
[8] T. Ohta, A. Bostwick, T. Seyller, K. Horn, and E. Rotenberg, Science **313**, 951 (2006); A. Bostwick, T. Ohta, T. Seyller, K. Horn, and E. Rotenberg, Nat. Phys. **3**, 36 (2007).
[9] We take data for the real and imaginary parts of the permittivity of Si from Ref. 10. The imaginary part is substantial only for $\omega > 1.5$ eV, so we approximate Im $\epsilon_{Si}(\omega < 1.5\text{eV}) \approx 0$. The permittivity of SiO_2 is nearly dispersionless in this frequency range (Ref. 11), so we take the SiO_2 dielectric constant as $\varepsilon_{SiO_2} = 3.9$. SiC has some dispersion for these frequencies[12] but the imaginary part is negligible so we assume Im $\epsilon_{SiC}(\omega) \approx 0$.
[10] J. Leng, J. Opsal, H. Chu, M. Senko, and D. E. Aspnes, Thin Solid Films **313-314**, 132 (1998).
[11] H. F. Wolf, *Silicon Semiconductor Data* (Pergamon, Oxford, 1969), 602ff.
[12] M. Kildemo, Thin Solid Films **455-456**, 187 (2004).
[13] L. A. Falkovsky and A. A. Varlamov, e-print arXiv:cond-mat/0606800.
[14] J. Nilsson, A. H. Castro Neto, F. Guinea, and N. M. R. Peres, Phys. Rev. Lett. **97**, 266801 (2007).
[15] D. S. L. Abergel and V. I. Fal'ko, Phys. Rev. B **75**, 155430 (2007).
[16] P. Blake, E. W. Hill, A. H. Castro Neto, K. S. Novoselov, D. Jiang, R. Yang, T. J. Booth, and A. K. Geim, Appl. Phys. Lett. **91**, 063124 (2007).
[17] C. Berger, Z. Song, T. Li, X. Li, A. Y. Ogbazghi, R. Feng, Z. Dai, A. N. Marchenkov, E. H. Conrad, P. N. First, and W. A. de Heer, J. Phys. Chem. B **108**, 19912 (2004).